

# GENERALIZED SENSITIVITY FUNCTIONS FOR SIZE-STRUCTURED POPULATION MODELS

DUSTIN D. KECK\* AND DAVID M. BORTZ\*<sup>†</sup>

**Abstract.** Size-structured population models provide a popular means to mathematically describe phenomena such as bacterial aggregation, schooling fish, and planetesimal evolution. For parameter estimation, generalized sensitivity functions (GSFs) provide a tool that quantifies the impact of data from specific regions of the experimental domain. These functions help identify the most relevant data subdomains, which enhances the optimization of experimental design. To our knowledge, GSFs have not been used in the partial differential equation (PDE) realm, so we provide a novel PDE extension of the discrete and continuous ordinary differential equation (ODE) concepts of Thomaseth and Cobelli and Banks et al. respectively. We analyze the GSFs in the context of size-structured population models, and specifically analyze the Smoluchowski coagulation equation to determine the most relevant time and volume domains for three, distinct aggregation kernels. Finally, we provide evidence that parameter estimation for the Smoluchowski coagulation equation does not require post-gelation data.

**1. Introduction.** General structured population models provide a link from the individuals in a population to the population processes [18, 19, 37]. A popular example, size-structured population models describe the distribution of individuals throughout varying size classes [13, 16]. Typical ODE based population models make a number of simplifying assumptions, a major one of which presumes homogeneity of the individuals' physical structure across the entire population. One effort to relax the homogeneity assumption resulted in the creation of age-structured population models which account for the effects of differing ages amongst the individuals comprising the population. Unfortunately, for some systems, age does not comprise the most influential physical attribute, but in many of these cases, size-structured population models do provide an adequate structuring of the population [14].

Size-structured population models often include an unknown parameter (or a set of unknown parameters). The value of this parameter is estimated via the inverse problem of parameter estimation based on experimental data. With a goal of optimizing the experiments, we seek to sample from domains which contain the most relevant information regarding the parameter estimation. Generalized sensitivity functions provide a tool which quantifies the importance of specific regions of a domain to the parameter of interest. Previous studies, such as cardiovascular regulation [8, 21, 22], HIV modeling [15], and HTLV-1 transactivation simulation [12], have applied the generalized sensitivity functions to ordinary differential equations. We denote these ODE-based GSFs as OGSFs. With our emphasis on size-structured population models, the primary goal of our work is to extend the concepts of OGSFs to the application of generalized sensitivity functions to PDEs, which we denote as PGSFs.

Thomaseth and Cobelli introduced the concept of OGSFs in [36]<sup>1</sup> and Batzel et al. recast the OGSFs into a probabilistic setting [9]. In a series of studies, Banks et al. [4, 6, 5] further develop the OGSF concept.. In particular, the work by Banks, Dediu, and Ernstberger [5] compares traditional sensitivity functions (TSFs) with OGSFs (in the context of general nonlinear ODEs) and highlights the potential utili-

\*Applied Mathematics, University of Colorado, Boulder, CO 80309-0526

<sup>†</sup>Corresponding author (dmbortz@colorado.edu)

<sup>1</sup>Note that in the original Thomaseth and Cobelli work, the functions are simply called GSFs (not OGSFs), since the authors are only considering ODE-based models.

ties of OGSFs. In [5], the authors also warn that OGSFs possess a potential weakness, which they denote as the *forced-to-one artifact* (discussed in Section 2). Then Banks, Davidian, Samuels, and Sutton [4] expand the results in [5] by introducing methodology for choosing between TSFs and OGSFs. Later, Banks, Dediu, Ernstberger, and Kappel [6] extend the OGSFs to a continuous setting and demonstrate the value of the OGSFs in the context of optimal experimental design.

As a case study for our extension of OGSFs to the PDE context, we apply our PGSFs to the Smoluchowski coagulation equation. This model for size-structured populations arises in the study of organic phenomena such as bacterial growth [10], marine snow [23], algal blooms [1, 2, 32], and schooling fish [30] and inorganic phenomena such as powder metallurgy [24], astronomy [25, 26, 27, 33], aerosols [17], irradiation of metals [35], and meteorology [31]. For our study, we determine the time and volume subdomains, which we denote  $\mathcal{D}^*$ , of greatest relevance to the estimate of the constant parameter in three coagulation kernels. In Section 2, we summarize the original work on OGSFs and the extensions to it. We then make a further extension of OGSFs to PGSFs for implementation on size-structured population models. In Section 3, we discuss the details of how we implement the PGSFs with respect to the Smoluchowski coagulation equation. In Section 4, we provide our results for each of three coagulation kernels. Finally in Section 5, we summarize the conclusions we have drawn from this study and discuss future directions for this research.

**2. Generalized sensitivity functions Theory.** Given a domain  $\mathcal{D}$  for the independent variables, the PGSFs will allow us to identify a subregion  $\mathcal{D}^* \subset \mathcal{D}$ , containing the information necessary to make the most accurate parameter estimates. The OGSFs and PGSFs vary from the TSFs<sup>2</sup> in the sense that the OGSFs and PGSFs do not depend on specific data realizations, which we explain in more detail in Section 2.1. When Thomaseth and Cobelli introduced the OGSFs in [36], they argued that the subdomain over which the OGSFs most rapidly increase to one contains the most relevant information for the parameter of interest. Then in [6], Banks et al. provide evidence that subdomains over which the OGSFs most rapidly decrease (indicating a high correlation between multiple parameters) also contain high information content.

In addition to the OGSFs, Thomaseth and Cobelli provide a related tool, the incremental (O)GSF, which computes the information at a given time point informing the value of a parameter estimate [36]. As advocated by the authors, the OGSFs and the incremental OGSFs should be regarded as complementary to one another. To demonstrate the complementary characteristics of OGSFs and incremental OGSFs, Thomaseth and Cobelli present an example where the plots of the OGSFs suggest an optimal  $\mathcal{D}^*$ . Banks et al. define a related quantity, the time derivative of the OGSFs, which plays the role of an incremental GSF when the OGSF is defined over continuous time (see a similarly complementary role to the continuous OGSFs).

As mentioned in Section 1, one weakness of generalized sensitivity functions is the so called *forced to one artifact* (FTOA). As addressed at length by Banks, Dediu, and Ernstberger in [5], plots of the OGSFs vary with changes in  $\mathcal{D}$ . Regardless of the choice of domain, by definition, the OGSFs and PGSFs will attain a value of one at the independent variables' maximum values in  $\mathcal{D}$ . Therefore, if  $\mathcal{D}$  possesses insufficient maximum values, the generalized sensitivity functions may provide misleading information about  $\mathcal{D}^*$  because they were (by definition) forced to a value of one on the upper bound of the domain. A strategy to counter this weakness [6] is to check

---

<sup>2</sup>For a summary of TSFs, see Stanley and Stewart [34].

that the time derivative of the OGSFs approaches zero within the original choice of  $\mathcal{D}$ . If it does not, we extend  $\mathcal{D}$  until the derivative does satisfy this criteria.

In Section 2.1, we summarize Thomaseth's and Cobelli's and Banks et al.'s development of the discrete and continuous OGSFs, respectively. In Section 2.2, we extend these previous works to the continuous PGSFs setting necessary for parameter estimation in size-structured population, PDE models. Finally, in Section 2.3, we propose mathematical criteria for determining  $\mathcal{D}^*$ .

**2.1. ODE-Based GSFs (OGSF).** In this section, we summarize the theory introduced by Thomaseth and Cobelli in [36] and Banks et al. in [4, 6, 5]. We provide this summary as convenient setting for introducing much of the notation and many of the definitions needed throughout this work.

First, we represent the system under consideration as a nonlinear regression function  $f(t; \theta)$  with  $t$  representing the sole independent variable and with  $\theta = [\theta_1, \theta_2, \dots, \theta_L]^T$  representing the parameter column vector with dimension  $L$ .<sup>3</sup> Then we represent the measurements with noise as

$$(2.1) \quad y(t) = f(t; \theta) + \epsilon(t),$$

where  $\epsilon(t)$  is the measurement noise. We assume an independent identically distributed noise distribution with zero mean and with known (but possibly time varying) variance,  $\sigma^2(t)$ . We also assume the existence of a true parameter vector  $\theta_0$ . When the observation times are discrete (as in [36]), the generalized sensitivity is defined as

$$(2.2) \quad \begin{aligned} \mathbf{gs}(t_k) = \sum_{i=1}^k \left\{ \left( \left[ \sum_{j=1}^{N_t} \frac{1}{\sigma^2(t_j)} \nabla_{\theta} f(t_j; \theta_0) \nabla_{\theta} f(t_j; \theta_0)^T \right]^{-1} \frac{\nabla_{\theta} f(t_i; \theta_0)}{\sigma^2(t_i)} \right) \right. \\ \left. \bullet \nabla_{\theta} f(t_i; \theta_0) \right\}, \end{aligned}$$

where  $\bullet$  indicates a Hadamard product and  $N_t$  is the number of timepoints. In the appendix to [36], the authors also introduce the incremental OGSFs defined as

$$\mathbf{gs}_{inc}(t_k) = \mathbf{gs}(t_k) - \mathbf{gs}(t_{k-1}),$$

yielding

$$(2.3) \quad \begin{aligned} \mathbf{gs}_{inc}(t_k) = \left( \left[ \sum_{j=1}^{N_t} \frac{1}{\sigma^2(t_j)} \nabla_{\theta} f(t_j; \theta_0) \nabla_{\theta} f(t_j; \theta_0)^T \right]^{-1} \frac{\nabla_{\theta} f(t_k; \theta_0)}{\sigma^2(t_k)} \right) \\ \bullet \nabla_{\theta} f(t_k; \theta_0). \end{aligned}$$

With this definition (2.3), one can calculate the contribution of the partial derivative at a specific point,  $t_k$ , rather than sum all contributions at times up to and including  $t_k$ .

Banks et al. developed a continuous version of the generalized sensitivity functions

$$(2.4) \quad \mathbf{gs}(t; \theta) = \int_0^t \left( F(\bar{t}; \theta)^{-1} \frac{1}{\sigma^2(s)} \nabla_{\theta} f(s; \theta_0) \right) \bullet \nabla_{\theta} f(s; \theta_0) dP(s), \quad t \in [0, \bar{t}].$$

---

<sup>3</sup> Note that bold typeface indicates a vector quantity.

where  $F(\bar{t}; \boldsymbol{\theta})$  represents the generalized Fisher information matrix [7]

$$F(\bar{t}; \boldsymbol{\theta}) := \int_0^{\bar{t}} \frac{1}{\sigma^2(s)} \nabla_{\boldsymbol{\theta}} f(s; \boldsymbol{\theta}) \nabla_{\boldsymbol{\theta}} f(s; \boldsymbol{\theta})^T dP(s).$$

As a tool to prevent misleading conclusions from a potential FTOA, Banks et al. further introduce the time derivative of  $gs(t; \boldsymbol{\theta})$

$$(2.5) \quad \frac{\partial}{\partial t} gs(t; \boldsymbol{\theta}) := \left( F(\bar{t}; \boldsymbol{\theta})^{-1} \frac{1}{\sigma^2(s)} \nabla_{\boldsymbol{\theta}} f(s; \boldsymbol{\theta}_0) \right) \bullet \nabla_{\boldsymbol{\theta}} f(s; \boldsymbol{\theta}_0).$$

In our subsequent work, we denote this quantity (2.5) as  $gs_{RIA}(t; \boldsymbol{\theta}) = \frac{\partial}{\partial t} gs(t; \boldsymbol{\theta})$ , i.e., the *rate of information acquisition* (RIA) at a specific point in  $\mathcal{D}$ .

**2.2. Continuous PDE-Based GSFs (PGSF).** In the OGSFs studies, the nonlinear regression function,  $f(t; \boldsymbol{\theta})$ , contains one independent variable, and a vector of parameters. For general size-structured population, continuous PDE models, we adapt the nonlinear regression function to depend on a column vector of independent variables, which we denote as  $\mathbf{r} = [r_1, r_2, \dots, r_{N_r}]^T$  with dimension  $N_r$ . For example, in the analysis of the OGSFs in Section 2.1,  $N_r = 1$  and  $r_1 = t$ , whereas with the Smoluchowski coagulation PDE,  $N_r = 2$  and  $[r_1, r_2] = [t, x]$ . Without loss of generality, we also let  $r_i \in [0, \bar{r}_i]$  for each  $i \in [1, 2, \dots, N_r]$ , where  $\bar{r}_i$  represents the maximum values of each independent variable respectively, and we denote the vector of maximum independent variable values  $\bar{\mathbf{r}} = [\bar{r}_1, \bar{r}_2, \dots, \bar{r}_{N_r}]^T$ . From the continuous OGSFs defined by Banks et al. in [6], we can then make the straight forward extension for the Fisher information matrix

$$F(\bar{\mathbf{r}}; \boldsymbol{\theta}) := \int_0^{\bar{r}_{N_r}} \int_0^{\bar{r}_{N_r-1}} \dots \int_0^{\bar{r}_1} \frac{1}{\sigma^2(\mathbf{r})} \nabla_{\boldsymbol{\theta}} f(\mathbf{r}; \boldsymbol{\theta}) \nabla_{\boldsymbol{\theta}} f(\mathbf{r}; \boldsymbol{\theta})^T dr_1 dr_2 \dots dr_{N_r},$$

and a continuous PGSF,

$$gs(\mathbf{r}; \boldsymbol{\theta}) = \int_0^{r_{N_r}} \int_0^{r_{N_r-1}} \dots \int_0^{r_1} \frac{1}{\sigma^2(\mathbf{r})} \left( F(\bar{\mathbf{r}}; \boldsymbol{\theta})^{-1} \frac{1}{\sigma^2(\mathbf{r})} \nabla_{\boldsymbol{\theta}} f(\mathbf{r}; \boldsymbol{\theta}_0) \right) \bullet \nabla_{\boldsymbol{\theta}} f(\mathbf{r}; \boldsymbol{\theta}_0) dr_1 dr_2 \dots dr_{N_r} \quad \boldsymbol{\theta} \in \mathbb{R}^L.$$

We also extend (2.5) to a *rate of information acquisition* (RIA) for a PGSF

$$gs_{RIA}(\mathbf{r}; \boldsymbol{\theta}) = \frac{\partial^{N_r}}{\partial r_{N_r} \partial r_{N_r-1} \dots \partial r_1} gs(\mathbf{r}; \boldsymbol{\theta}) := \left( F(\bar{\mathbf{r}}; \boldsymbol{\theta})^{-1} \frac{1}{\sigma^2(\mathbf{r})} \nabla_{\boldsymbol{\theta}} f(\mathbf{r}; \boldsymbol{\theta}_0) \right) \bullet \nabla_{\boldsymbol{\theta}} f(\mathbf{r}; \boldsymbol{\theta}_0).$$

In this work, we examine size-structured populations in a general context, therefore we assume a constant variance of one and normal error distribution for all measurements. Furthermore, for our purposes, we adapt the nonlinear regression function so that  $f$  depends on two variables,  $t$  and  $x$ , and one parameter,  $\alpha$ , so that

$$(2.6) \quad gs(t, x; \alpha) = \frac{\int_0^t \int_0^x \left( \frac{\partial f}{\partial \alpha} \right)^2 dr ds}{\int_0^{\bar{t}} \int_0^{\bar{x}} \left( \frac{\partial f}{\partial \alpha} \right)^2 dr ds},$$

where  $\bar{t}$  and  $\bar{x}$  represents the maximum values of time and volume respectively. Also, for the rate of information acquisition,

$$(2.7) \quad \begin{aligned} gs_{RIA}(t, x; \alpha) &:= \frac{\partial^2}{\partial t \partial x} [gs(t, x; \alpha)] = \frac{\partial^2}{\partial t \partial x} \left[ \frac{\int_0^t \int_0^x \left( \frac{\partial f}{\partial \alpha} \right)^2 dr ds}{gs(\bar{t}, \bar{x}; \alpha)} \right] \\ &= \frac{\left( \frac{\partial f(t, x; \alpha)}{\partial \alpha} \right)^2}{gs(\bar{t}, \bar{x}; \alpha)}. \end{aligned}$$

**2.3. Determining the optimum subdomain,  $\mathcal{D}^*$ .** In [36], Thomaseth and Cobelli only offer a visual analysis of how we can apply the OGSFs to determine  $\mathcal{D}^*$ . In [6], Banks et al. propose a mathematical implementation to determine the upper bound of  $\mathcal{D}^*$  by bounding the TSFs variation. In this section, we offer a quantitative means for computing the lower and upper bounds of an optimal  $\mathcal{D}^*$ . To determine the lower ends of  $\mathcal{D}^*$ , we consider a level curve that represents a fraction of the maximum RIA. Then to determine the upper ends of  $\mathcal{D}^*$ , we consider a second level curve that represents the points where the PGSFs approach a value of one.

First, we consider the RIA to determine the lower ends of  $\mathcal{D}^*$ . In the analysis that follows, we assume only two independent variables and one parameter with  $\mathcal{D} = [\underline{t}, \bar{t}] \times [\underline{x}, \bar{x}]$ .<sup>4</sup> We define the maximum  $gs_{RIA}$  as

$$\overline{gs}_{RIA} = \max_{(t, x) \in \mathcal{D}} \{ |gs_{RIA}(t, x; \alpha)| \}.$$

Then we denote a fraction  $\gamma \in (0, 1)$  of  $\overline{gs}_{RIA}$  and define the level curve,  $\Gamma_\gamma$ , where

$$\Gamma_\gamma = \{ (t, x) \mid |gs_{RIA}(t, x; \alpha)| = \gamma \overline{gs}_{RIA} \},$$

and from that level curve, we find the minimum values of  $x$  and  $t$ , which we denote  $x_*$  and  $t_*$ , where  $x_* = \min_x \Gamma_\gamma$  and  $t_* = \min_t \Gamma_\gamma$ .

Second, we consider the PGSFs to determine the upper ends of  $\mathcal{D}^*$ . We let  $\rho$  represent the proximity to one that we desire, and define the level curve,  $\Gamma^\rho$ , where

$$\Gamma^\rho = \{ (t, x) \mid |1 - gs(t, x; \alpha)| = \rho \}.$$

Note that any point in the set  $\Gamma^\rho$  provides a satisfactory upper bound on  $\mathcal{D}^*$ . To determine a range of upper bounds depending on which independent variable costs more in terms of gathering data, we consider  $x^* = \min_x \Gamma^\rho$  with its dependent  $t(x^*)$ , and  $t^* = \min_t \Gamma^\rho$  with its dependent  $x(t^*)$ . We denote the optimum subdomain as  $\mathcal{D}_x^*$ , where

$$\mathcal{D}_x^* = [t_*, t(x^*)] \times [x_*, x^*],$$

when high resolution data in  $x$  is more expensive. Conversely, when high resolution data in  $t$  is more expensive, we denote the optimum subdomain as  $\mathcal{D}_t^*$ , where

$$\mathcal{D}_t^* = [t_*, t^*] \times [x_*, x(t^*)].$$

---

<sup>4</sup>The inclusion of additional independent variables and parameters is straightforward.

### 3. Application of PGSEs to the Smoluchowski coagulation equation.

Our extension to PGSEs allows us to apply it to the Smoluchowski coagulation equation with one parameter of interest, the aggregation kernel constant. In the early 1900's, van Smoluchowski developed a model to study the coagulation of colloids [38, 39],

$$(3.1) \quad \frac{d}{dt}f_k = \frac{1}{2} \sum_{i+j=k} K(i, j)f_i f_j - \sum_i K(i, k)f_i f_k,$$

where  $f_k$  represents the number density of aggregates of volume  $k$ , and  $K(i, j)$  is the aggregation kernel denoting the rate at which aggregates of size  $i$  and  $j$  form a combined aggregate of size  $i + j$  [10, 38, 39]. Müller subsequently extended this model to a continuous PDE [20, 29]

$$(3.2) \quad \begin{aligned} \partial_t f &= A(f), \quad (t, x) \in \mathbb{R}_+^2, \\ f(0) &= f_0, \quad x \in \mathbb{R}_+ \end{aligned}$$

where each aggregate is classified solely by its volume  $x > 0$ , and  $f = f(t, \cdot)$  represents the continuous size distribution function of aggregates at time  $t \geq 0$ . The coagulation term is

$$(3.3) \quad \begin{aligned} A(f) &= A_{in}(f) - A_{out}(f) \\ &= \frac{1}{2} \int_0^x K(y, x-y)f(t, y)f(t, x-y)dy \\ &\quad - f(x) \int_0^\infty K(x, y)f(y)dy \end{aligned}$$

where  $K(x, y)$  is the aggregation kernel indicating the rate at which aggregates of volumes  $x$  and  $y$  join together creating an aggregate of volume  $x + y$ . Notice the first integral,  $A_{in}(f)$ , describes aggregates with volumes  $y$  and  $x - y$  aggregating to a combined volume  $x$ , and the second integral,  $A_{out}(f)$ , models interactions between the aggregate of volume  $x$  with all other aggregates of volume  $y$  forming an aggregate of volume  $x + y$ . Also, note that the aggregation kernel  $K(x, y)$  is positive and symmetric

$$0 < K(x, y) = K(y, x), \quad (x, y) \in \mathbb{R}_+^2,$$

as well as homogeneous, which in this field, is defined as

$$(3.4) \quad K(\lambda x, \lambda y) = \lambda^m K(x, y), \quad \lambda > 0, m \geq 0, x, y < \infty.$$

Because only aggregation is considered, the total number of particles decreases with each coagulation event.

In practice, when we model experimental data, we often find that the measurements made by experimental devices can produce heteroscedasticity in the data, i.e., data with non-constant variation. An advantage of the OGSFs, in both the discrete and continuous versions, lies in their incorporation of a weighted residual sum of squares (WRSS), which allows for differing variance. In this context, the OGSFs give a greater weight to measurements with smaller variation.

Additionally, when we know specifically how the variance differs, we transform the model to overcome heteroscedasticity. For example, with many experimental devices, the measurement error grows with the size of the quantity measured resulting in a log-normal error distribution (as described in [11] and utilized in [10]). With a log-normal error distribution, the analog of (2.1) would be

$$\log [y(t)] = \log [f(t, \boldsymbol{\theta})] + \epsilon ,$$

where  $\epsilon$  has a normal distribution with zero mean and variance,  $\sigma^2$ . For the purposes of this paper, we will only consider constant variance.

To illustrate an application of the PGSFs to the continuous model in (3.3), we choose three coagulation kernels, the constant, the additive, and the multiplicative, for which known solutions to (3.2) exist. In Section 3.1, we list the three solutions with proper placement of the constant parameter,  $\alpha$ . Additionally, we justify our choice of minimums for  $\mathcal{D}$ . Then in Section 3.2, we discuss the benefits and drawbacks of different choices for the order of summation when calculating the PGSFs.

**3.1. Set up.** In Table 3.1, we list the three kernels studied in this work and the source of the known solution. Note that analytical solutions presented in the literature commonly assume a constant,  $\alpha = 1$ , in the aggregation kernels. We aim to identify the value of  $\alpha$ , so we incorporate it as the general constant.

|                | $K(x, y)$       | $f(t, x; \alpha)$ for general constant,<br>$\alpha \in \mathbb{R}_+ < \infty$  | Source                 |
|----------------|-----------------|--|------------------------|
| Constant       | $\alpha$        | $f(t, x; \alpha) = \left(\frac{2}{\alpha t}\right)^2 e^{\frac{-2x}{\alpha t}},$<br>for $x \in [0, \infty), \alpha t \in (0, \infty)$ | Aldous [3]             |
| Additive       | $\alpha(x + y)$ | $\frac{1}{\sqrt{2\pi}} x^{-3/2} (e^{-\alpha t}) e^{-x/(2e^{2\alpha t})},$<br>for $x \in (0, \infty), \alpha t \in [0, \infty)$       | Menon<br>and Pego [28] |
| Multiplicative | $\alpha xy$     | $\frac{1}{\sqrt{2\pi}} x^{-5/2} e^{-(1-\alpha t)^2 x/2},$<br>for $x \in (0, \infty), \alpha t \in [0, 1)$                            | Menon<br>and Pego [28] |

Table 3.1: Solutions to the Smoluchowski coagulation equation

The PGSFs are defined on a domain which starts at a point  $\mathbf{0} \in \mathbb{R}^N$ . For our purposes, the PGSFs incorporate  $\left(\frac{\partial f}{\partial \alpha}\right)^2$ , so when we examine the lower ends of  $\mathcal{D}$ , we must consider the limit as  $t, x \rightarrow 0^+$  of  $\left(\frac{\partial f}{\partial \alpha}\right)^2$ . As an example, consider the constant kernel where

$$\frac{\partial f}{\partial \alpha} = \frac{8}{t^2 \alpha^3} e^{\frac{-2x}{\alpha t}} \left[ \frac{x}{t\alpha} - 1 \right].$$

Choosing the path along  $x = 0$  demonstrates an infinite limit,

$$\begin{aligned} \lim_{(t,0) \rightarrow (0^+,0^+)} \left(\frac{\partial f}{\partial \alpha}\right)^2 &= \lim_{(t,0) \rightarrow (0^+,0^+)} \frac{64}{t^4 \alpha^6} e^{\frac{-4x}{\alpha t}} \left[ \frac{x}{t\alpha} - 1 \right]^2 \\ (3.5) \qquad \qquad \qquad &= \lim_{(t,0) \rightarrow (0^+,0^+)} \frac{64}{t^4 \alpha^6}. \end{aligned}$$

The infinite limit in (3.5) helps guide our choice of  $\underline{t} = 0.2$  because it ensures our PGSFs calculations remain within computer precision. Similar analysis leads to

choices of  $\underline{x} = 0.1$  for both the additive kernel and the multiplicative kernel. In Appendix A, we present similar calculations in detail for all three kernels, justifying the choice of the lower bounds in each case.

**3.2. Summation choices for calculating PGSEs.** We note that in (2.6), one is faced with a choice of which variable is summed first. This choice is not encountered in the OGSFs context. To calculate the generalized sensitivity, we can calculate the numerator in (at least) three ways.

One possible choice, which we designate as the *Simultaneously Incremental* (SI) method, involves summing along the spatial axis to  $x_s$  with  $s = 1, \dots, N_x$  and then incrementing time. For the SI method,

$$(3.6) \quad \begin{aligned} gs_{SI}(t_k, x_s; \alpha) &= \frac{\int_0^{t_k} \int_0^{x_s} \left( \frac{\partial f}{\partial \alpha} \right)^2 dx dt}{gs(\bar{t}, \bar{x}; \alpha)} \\ &\approx \frac{\sum_{i=1}^k \sum_{j=1}^s \left( \frac{\partial f}{\partial \alpha}(t_i, x_j; \alpha) \right)^2 \Delta x_j \Delta t_i}{gs(\bar{t}, \bar{x}; \alpha)}, \end{aligned}$$

where  $\Delta x_j = x_{j+1} - x_j$  and  $\Delta t_j = t_{j+1} - t_j$ , where  $N_x$  represents the number of volume points. Unless otherwise specified, we space our grids uniformly. Note that in (3.6), the order of summation does not matter.

We designate the second method, the *All Size, Incremental in Time* (ASIT) method, with which we sum along the entire size-axis before we increment time. For the ASIT method, we denote  $(t_k, x_s) = (t, x)_i$  such that  $i = s + (k - 1)N_x$  with  $k = 1, 2, \dots, N_t$  and  $s = 1, 2, \dots, N_x$ . Then for the ASIT method,

$$\begin{aligned} gs_{ASIT}((t, x)_i; \alpha) &= gs_{ASIT}(t_k, x_s; \alpha) = \frac{\int_0^{t_k} \int_0^{x_s} \left( \frac{\partial f}{\partial \alpha} \right)^2 dx dt}{gs(\bar{t}, \bar{x}; \alpha)} \\ &\approx \frac{\sum_{j=1}^i \left( \frac{\partial f}{\partial \alpha}((t, x)_j; \alpha) \right)^2 \Delta x_j \Delta t_j}{gs(\bar{t}, \bar{x}; \alpha)}. \end{aligned}$$

Lastly, we designate the third method, the *All Time, Incremental in Size* (ATIS) method, with which we sum along the entire time-axis before we increment the size dimension. In this case, we denote  $(t_k, x_s) = (t, x)_j$  such that  $j = k + (s - 1)N_t$  with  $k = 1, 2, \dots, N_t$  and  $s = 1, 2, \dots, N_x$ . Therefore

$$\begin{aligned} gs_{ATIS}((t, x)_j; \alpha) &= gs_{ATIS}(t_k, x_s; \alpha) = \frac{\int_0^{t_k} \int_0^{x_s} \left( \frac{\partial f}{\partial \alpha} \right)^2 dx dt}{gs(\bar{t}, \bar{x}; \alpha)} \\ &\approx \frac{\sum_{i=1}^j \left( \frac{\partial f}{\partial \alpha}((t, x)_i; \alpha) \right)^2 \Delta x_j \Delta t_j}{gs(\bar{t}, \bar{x}; \alpha)}. \end{aligned}$$

For all three methods, we compute the denominator of our generalized sensitivity,

$$\begin{aligned} gs(\bar{t}, \bar{x}; \alpha) &= \int_0^{\bar{t}} \int_0^{\bar{x}} \left( \frac{\partial f}{\partial \alpha}(t, x; \alpha) \right)^2 dx dt \\ &= \sum_{i=1}^{N_t-1} \int_{t_i}^{t_{i+1}} \sum_{j=1}^{N_x-1} \int_{x_j}^{x_{j+1}} \left( \frac{\partial f}{\partial \alpha}(t, x; \alpha) \right)^2 dx dt \end{aligned}$$



$$(3.7) \quad \approx \sum_{i=1}^{N_t-1} \sum_{j=1}^{N_x-1} \left( \frac{\partial f}{\partial \alpha}(t_i, x_j; \alpha) \right)^2 \Delta x_j \Delta t_i.$$

In Section 4, we offer justification for calculating the PGSFs via the SI method rather than via either the ASIT or ATIS methods.

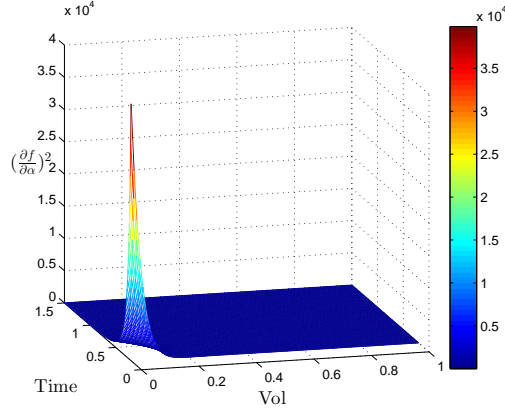
**4. Determining  $\mathcal{D}^*$  for the Smoluchowski coagulation equation with PGSFs.** In order to apply the PGSFs concept to the Smoluchowski coagulation equation, we make several decisions. First, we choose three aggregation kernels, constant, additive, and multiplicative, for which known solutions exist. Next we choose  $\mathcal{D}$  and the number of points on our grid. These choices need to provide enough information and enough resolution to extract a meaningful  $\mathcal{D}^*$ . We provide the details of the impacts of these choices later in this section. Finally, in order to compute the PGSFs, we choose the advocate for one of the three summation orders described in Section 3.2.

In the use of GSFs, a natural question concerns choosing the overall domain  $\mathcal{D}$ . For all three kernels, to choose the lower bounds ( $\underline{x}$  and  $\underline{t}$ ) of  $\mathcal{D}$ , we face the following dilemma concerning the FTOA.<sup>5</sup> After we determine  $\underline{x}$  and  $\underline{t}$ , determining  $\bar{x}$  and  $\bar{t}$  in conjunction with grid spacing also presents difficulties. If we space the grid too widely, the PGSFs reach one on the first step, which does not provide a meaningful resolution. Furthermore, if we use maximum values for  $\mathcal{D}$  that are too small, we face a potential FTOA as described in Section 2. To avoid this artifact, we examine the PGSFs curves and the RIA curves to ensure that the PGSFs curves stabilize at one well before the maximum domain limits and to confirm that the RIA stabilizes near zero. If we do not achieve both of those criteria, we need to increase  $\bar{x}$  or  $\bar{t}$  until we do. For all three kernels that we study, the PGSFs curves in Figures 4.2a, 4.3a, and 4.4a, do stabilize at one before  $\bar{x}$  and  $\bar{t}$ , and the RIA stabilizes near zero in Figures 4.2b, 4.3b, and 4.4b.

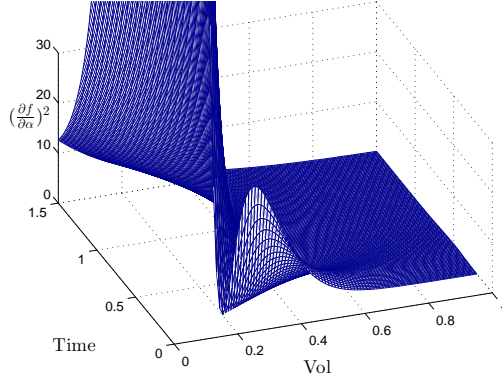
The primary purpose of applying PGSFs in our study is to determine the subdomains,  $\mathcal{D}^*$ , that contain the most important information relative to estimating the constant,  $\alpha$ . In our application of the PGSFs to the Smoluchowski coagulation equation, we incorporate one parameter, therefore  $\left( \frac{\partial f}{\partial \alpha} \right)^2$  provides the primary quantity of interest. As depicted in Figure 4.1a, for the constant kernel, we notice a large spike at small times and volumes. Then zooming in as depicted in Figure 4.1b, we notice more detail at volumes greater than approximately 0.2. The plots in Figure 4.1, do not clearly indicate the importance of the subdomain,  $x \in [0.2, 0.6]$ .

---

<sup>5</sup>Recall the FTOA is described in Section 3.1. We also expand upon this issue in Appendix A



(a) Entire range



(b) Zoomed in

Figure 4.1:  $\left(\frac{\partial f(t,x)}{\partial \alpha}\right)^2$  vs.  $x$  and  $t$  for  $K(x,y) = \alpha$ : In (a) we plot the entire range which illustrates the spike at small time and small volume points, and in (b) we illustrate more detail away from the spike.

Conversely, the PGSFs and RIA plots allows us to quantify the relative importance of all the contributions. Figure 4.2 reveals the PGSFs approach one and the rates of information acquisition approach zero well within  $\mathcal{D}$ . By implementing the mathematical strategy in Section 2.3, we compute the lower bounds,  $(t_*, x_*) = (0.2, 0)$ , from  $\Gamma_\gamma$  and the upper bounds, which range from  $(t(x^*), x^*) \approx (0.94, 0.11)$  to  $(t^*, x(t^*)) \approx (0.56, 0.48)$ , from  $\Gamma^\rho$ . We achieve these results (and the results for the other two kernels) by setting  $\Delta t = \Delta x = .01$ ,  $\gamma = 0.5$ , and  $\rho = 0.1$  and by implementing the SI method described in Section 3.2.

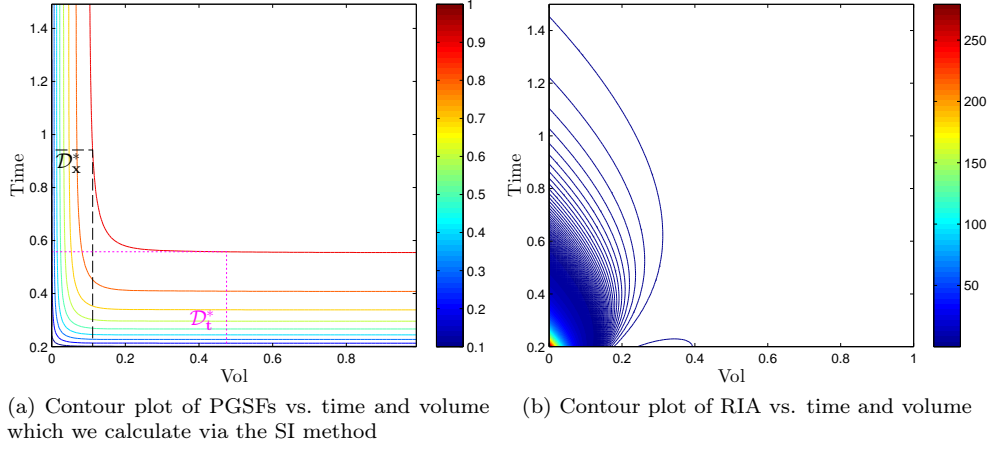


Figure 4.2: Generalized Sensitivity and RIA for the constant kernel - subregions where the largest rates of change occur as the PGSFs transition from zero to one indicate an approximate  $\mathcal{D}^*$ . The rectangles in (a) represent optimum subdomains,  $\mathcal{D}_x^*$  and  $\mathcal{D}_t^*$ , as summarized in Table 4.1.

We can determine  $\mathcal{D}^*$  for the additive and multiplicative kernels by performing similar assessments of the PGSFs plots (in Figures 4.3a and 4.4a) to ensure we avoid the FTOA. We then confirm that the rates approach zero in those subdomains in Figures 4.3b and 4.4b respectively. By implementing the mathematical strategy in Section 2.3 for the additive kernel, we compute the lower bounds,  $(t_*, x_*) = (0.42, 0.1)$ , and the upper bounds, which range from  $(t(x^*), x^*) \approx (4.27, 0.28)$  to  $(t^*, x(t^*)) \approx (2.69, 0.94)$ . For the multiplicative kernel, we compute the lower bounds,  $(t_*, x_*) = (0.24, 0.1)$ , and the upper bounds, which range from  $(t(x^*), x^*) \approx (0.92, 0.28)$  to  $(t^*, x(t^*)) \approx (0.76, 0.75)$ . We summarize  $\mathcal{D}^*$  for each aggregation kernel in Table 4.1.

| $K(x, y)$       | $\mathcal{D}_x^* = [t_*, t(x^*)] \times [x_*, x^*]$ | $\mathcal{D}_t^* = [t_*, t^*] \times [x_*, x(t^*)]$ | Gelation               |
|-----------------|---|---|------------------------|
| $\alpha$        | $[0.2, 0.94] \times [0, 0.11]$                      | $[0.2, 0.56] \times [0, 0.48]$                      |                        |
| $\alpha(x + y)$ | $[0.42, 4.27] \times [0.1, 0.28]$                   | $[0.42, 2.69] \times [0.1, 0.94]$                   |                        |
| $\alpha xy$     | $[0.24, 0.92] \times [0.1, 0.28]$                   | $[0.24, 0.76] \times [0.1, 0.75]$                   | $t = \frac{1}{\alpha}$ |

Table 4.1: Summary of  $\mathcal{D}^*$  when estimating the constant in three aggregation kernels for the Smoluchowski coagulation equation. We achieve these results by setting  $\Delta t = \Delta x = .01$ ,  $\gamma = 0.5$ , and  $\rho = 0.1$  and by implementing the SI method described in Section 3.2. The second column reflects an optimum subdomain when volume data is more costly and the third column denotes an optimum subdomain when the time data is more costly. Note that the time subdomain for the multiplicative kernel indicates that the pertinent information occurs prior to gelation.

The PGSFs for the multiplicative kernel provide another important result. It is

well known that *gelation* occurs for the multiplicative kernel<sup>6</sup>. When gelation occurs the system experiences growth rapid enough that aggregates with *infinite* volume develop in finite time [40]. Mass is not physically lost, but the aggregates with *infinite* volume possess fundamentally different mathematical properties than the individual aggregates that make up the gel. We direct the interested reader to [41], in which Ziff and Stell provide a thorough description of the implications of various assumptions on the post-gelation behavior of the solutions and of the moments. As summarized in Table 4.1, our results provide evidence that the pertinent information necessary for estimating the constant in  $K(x, y) = \alpha xy$  occurs well before gelation.

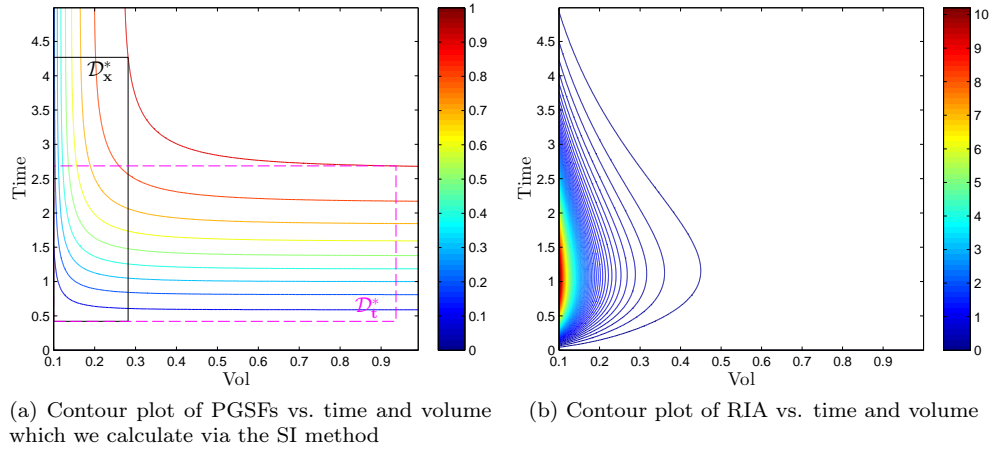


Figure 4.3: Generalized Sensitivity and RIA for the additive kernel - subregions where the largest rates of change occur as the PGSFs transition from zero to one indicate an approximate  $\mathcal{D}^*$ . The rectangles in (a) represent optimum subdomains,  $\mathcal{D}_x^*$  and  $\mathcal{D}_t^*$ , as summarized in Table 4.1.

<sup>6</sup>With the multiplicative kernel, gelation occurs at  $t = \frac{1}{\alpha}$ .

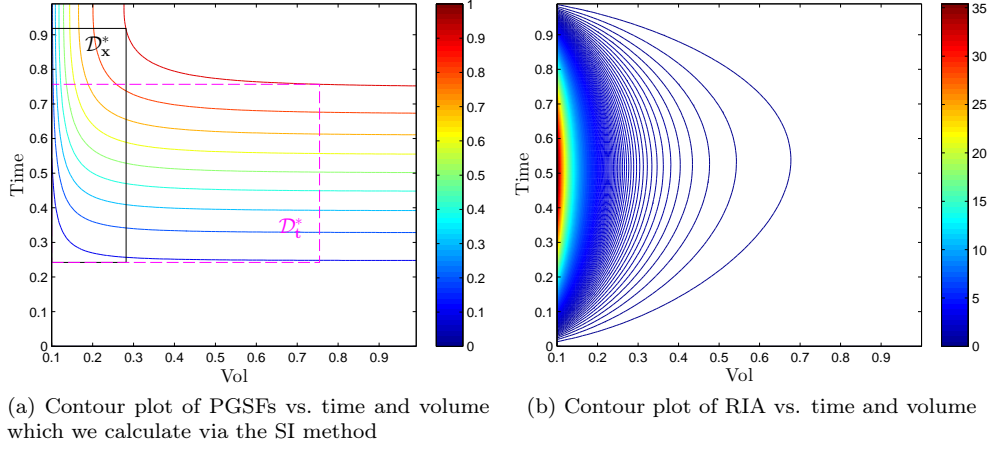


Figure 4.4: Generalized Sensitivity and RIA for the multiplicative kernel - subregions where the largest rates of change occur as the PGSFs transition from zero to one indicate an approximate  $\mathcal{D}^*$ . The rectangles in (a) represent optimum subdomains,  $\mathcal{D}_x^*$  and  $\mathcal{D}_t^*$ , as summarized in Table 4.1.

Finally, as described in Section 3.2, we examined three summation methods when calculating the PGSFs. We plot the constant kernel PGSFs for each of the three methods in Figure 4.5. The ASIT method indicates the approximate  $\bar{t}$  necessary for the generalized sensitivity to reach one, but it does not provide an obvious indication of  $\bar{x}$ . Conversely, the ATIS method indicates the necessary  $\bar{x}$  for the generalized sensitivity to reach one, but it does not provide useful information relative to the time domain. However, the SI method simultaneously illustrates a combination of the ASIT and ATIS methods and provides both time and volume indications of where the generalized sensitivity reaches one. We achieve similar results for the additive and multiplicative kernels. Note that regardless of the summation scheme we use, the RIA remains the same.

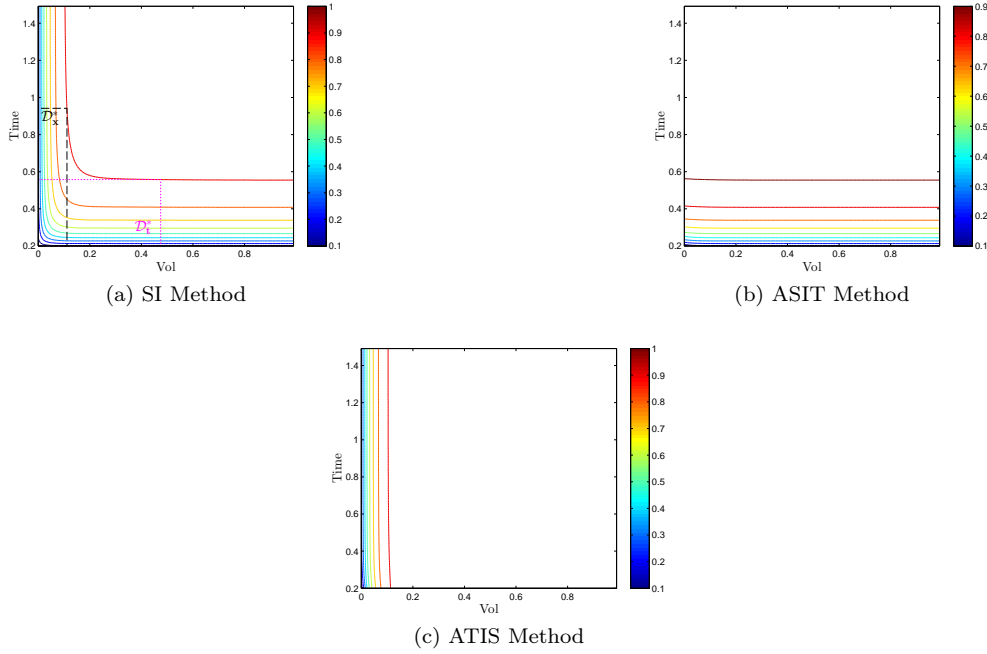


Figure 4.5: Comparison of the the three summation methods for calculating the PGSFs for the constant kernel: in (a), we sum along  $x$  to  $x_s$  and then increment time. In (b), we sum along  $x$  to  $x_{N_x}$  and then increment time. In (c), we sum along  $t$  to  $t_{N_t}$  and then increment volume. Note that the SI method illustrates a combination of the ASIT and ATIS methods providing both time and volume indications of where the generalized sensitivity reaches one on the same plot.

**5. Conclusions and Future Work.** In this work, we have extended the concepts of the ODE-based GSFs introduced by Thomaseth and Cobelli in [36], to the PDE-based GSFs. These PGSFs provide a framework for determining an optimum subdomain,  $\mathcal{D}^*$ , for size-structured population, PDE models. We then apply PGSFs to the Smoluchowski coagulation equation, a popular size-structured population model, to determine  $\mathcal{D}^*$  for parameter estimation in the constant, additive, and multiplicative kernels.

To accomplish the goal of determining optimal experimental domains, we offer a novel mathematical means of determining the entire  $\mathcal{D}^*$  from generalized sensitivity functions. Specifically for the Smoluchowski coagulation equation, we determine that pertinent information for estimating the constant parameter,  $\alpha$ , occurs in small volume subdomains. When time data costs less than volume data, we generally require no larger than  $x \approx 0.3$ . We require no larger than  $x \approx 0.94$  when time data is more costly than volume data. We also determine that the most relevant time information occurs early in a coagulation experiment. How early varies widely among the three kernels with maximum times ranging from 0.56 to 4.27. Our study also acknowledges the potential for a *force to one artifact*, FTOA, which is a known weakness of the generalized sensitivity functions. By addressing this weakness, we determine maxima in  $\mathcal{D}$  which eliminate the artifact. Finally, we also provide results which indicate

that all of the relevant time information for the multiplicative kernel occurs prior to gelation.

With our application to the Smoluchowski coagulation equation, we include only one parameter to estimate. Generally, PGSFs allows accounting for multiple parameters, and in our future work we aspire to study more sophisticated aggregation kernels which contain multiple parameters. As is popular in much of the literature, we will examine kernels of the form,  $K(x, y) = \alpha(x^\mu y^\nu + x^\nu y^\mu)$ .

Additionally, the results generated in Section 4 follow from inputting a specific true parameter. Clearly, altering that parameter could shift  $\mathcal{D}^*$ . As a future step, we aim to methodically study a range of true parameters and their respective optimum subdomains.

Lastly, in this work, we study the Smoluchowski coagulation equation, which models processes involving aggregation only. In the future, we would like to consider the Smoluchowski coagulation-fragmentation equation for which we would estimate both aggregation and fragmentation parameters.

**6. Acknowledgments.** This work was supported in part by the National Science Foundation grant DMS-1225878. We would also like to thank Dr. John Younger in the Department of Emergency Medicine at the University of Michigan for our discussions concerning experimental data.

#### REFERENCES

- [1] A. S. ACKLEH, *Parameter estimation in a structured algal coagulation-fragmentation model*, Nonlinear Anal., 28 (1997), pp. 837–854.
- [2] A. S. ACKLEH AND B. G. FITZPATRICK, *Modeling aggregation and growth processes in an algal population model: analysis and computations*, J. Math. Biol., 35 (1997), pp. 480–502.
- [3] D. J. ALDOUS, *Deterministic and Stochastic Models for Coalescence (Aggregation, Coagulation): A Review of the Mean-Field Theory for Probabilists*, Bernoulli, 5 (1999), pp. 3–48.
- [4] H. T. BANKS, M. DAVIDIAN, J. R. SAMUELS, AND K. L. SUTTON, *Chapter 11: Mathematical and Statistical Estimation Approaches in Epidemiology*, in Math. Stat. Estim. Approaches Epidemiol., G. Chowell, J. M. Hyman, L. M. A. Bettencourt, and C. Castillo-Chavez, eds., Springer Netherlands, Dordrecht, 2009, pp. 249–302.
- [5] H. T. BANKS, S. DEDIU, S. L. ERNSTBERGER, AND F. KAPPEL, *Sensitivity functions and their uses in inverse problems*, J. Inverse Ill-posed Probl. jiiip, 15 (2008), pp. 683–708.
- [6] ———, *Generalized sensitivities and optimal experimental design*, J. Inverse Ill-posed Probl., 18 (2010), pp. 25–83.
- [7] H. T. BANKS, K. HOLM, AND F. KAPPEL, *Comparison of Optimal Design Methods in Inverse Problems*, Inverse Probl., 27 (2011), p. 075002.
- [8] J. BATZEL, G. BASELLI, R. MUKKAMALA, AND K. H. CHON, *Modelling and disentangling physiological mechanisms: linear and nonlinear identification techniques for analysis of cardiovascular regulation*, Philos. Trans. A. Math. Phys. Eng. Sci., 367 (2009), pp. 1377–91.
- [9] J. J. BATZEL, F. KAPPEL, D. SCHNEDITZ, AND H. T. TRAN, *Cardiovascular and Respiratory Systems: Modeling, Analysis, and Control*, vol. 14, SIAM, 2007.
- [10] D. M. BORTZ, T. L. JACKSON, K. A. TAYLOR, A. P. THOMPSON, AND J. G. YOUNGER, *Klebsiella pneumoniae flocculation dynamics*, Bull. Math. Biol., 70 (2008), pp. 745–68.
- [11] R. J. CARROLL AND D. RUPPERT, *Transformation and Weighting in Regression*, Chapman and Hall, 1988.
- [12] A. CORRADIN, B. DI CAMILLO, V. CIMINALE, G. TOFFOLO, AND C. COBELLI, *Sensitivity analysis of retrovirus HTLV-1 transactivation*, J. Comput. Biol., 18 (2011), pp. 183–93.
- [13] J. M. CUSHING, *An Introduction to Structured Population Dynamics*, SIAM, Philadelphia, PA, 1987.
- [14] ———, *Some competition models for size-structured populations*, Rocky Mt. J. Math., 20 (1990), pp. 879–897.
- [15] J. DAVID, H. TRAN, AND H. T. BANKS, *HIV model analysis and estimation implementa-*

- tion under optimal control base treatment strategies, *Int. J. Pure Appl. Math.*, 57 (2009), pp. 357–392.
- [16] M. DOUMIC, P. MAIA, AND J. P. ZUBELLI, *On the calibration of a size-structured population model from experimental data.*, *Acta Biotheor.*, 58 (2010), pp. 405–13.
  - [17] R. L. DRAKE, *A General Mathematical Survey of the Coagulation Equation*, in *Top. Curr. Aerosol Res. (Part 2)*, G. M. Hidy and J. R. Brock, eds., vol. 3 of *International Reviews in Aerosol Physics and Chemistry*, Pergamon Press, New York, NY, 1972, pp. 201–376.
  - [18] M. R. EASTERLING, S. P. ELLNER, AND P. M. DIXON, *Size-specific sensitivity: applying a new structured population model*, *Ecology*, 81 (2000), pp. 694–708.
  - [19] B. EBENMAN AND L. PERSSON, eds., *Size-Structured Populations*, Springer Berlin Heidelberg, Berlin, Heidelberg, 1988.
  - [20] F. FILBET AND P. LAURENÇOT, *Numerical Simulation of the Smoluchowski Coagulation Equation*, *SIAM J. Sci. Comput.*, 25 (2004), p. 2004.
  - [21] M. FINK, J. BATZEL, AND F. KAPPEL, *Modeling the Human Cardiovascular Control Response to Blood Volume Loss Due to Hemorrhage*, *Biomed. Eng. (NY)*, L (2006), pp. 145–152.
  - [22] M. FINK, J. J. BATZEL, AND H. TRAN, *A respiratory system model: parameter estimation and sensitivity analysis.*, *Cardiovasc. Eng.*, 8 (2008), pp. 120–34.
  - [23] T. KJØRBOE, *Formation and fate of marine snow: small-scale processes with large-scale implications*, *Sci. Mar.*, 65 (2001), pp. 57–71.
  - [24] J. KUMAR, G. WARNECKE, M. PEGLOW, AND S. HEINRICH, *Comparison of numerical methods for solving population balance equations incorporating aggregation and breakage*, *Powder Technol.*, 189 (2009), pp. 218–229.
  - [25] M. H. LEE, *On the Validity of the Coagulation Equation and the Nature of Runaway Growth*, *Icarus*, 143 (2000), pp. 74–86.
  - [26] ———, *A survey of numerical solutions to the coagulation equation*, *J. Phys. A. Math. Gen.*, 34 (2001), pp. 10219–10241.
  - [27] J. MAKINO, T. FUKUSHIGE, Y. FUNATO, AND E. KOKUBO, *On the mass distribution of planetesimals in the early runaway stage*, *New Astron.*, 3 (1998), pp. 411–417.
  - [28] G. MENON AND R. L. PEGO, *Dynamical Scaling in Smoluchowski’s Coagulation Equations: Uniform Convergence*, *SIAM Rev.*, 48 (2006), p. 745.
  - [29] H. MÜLLER, *Zur allgemeinen Theorie der raschen Koagulation*, *Kolloidchem. Beihefte*, 27 (1928), pp. 257–311.
  - [30] H.-S. NIWA, *School size statistics of fish*, *J. Theor. Biol.*, 195 (1998), pp. 351–61.
  - [31] H. R. PRUPPACHER AND J. D. KLETT, *Microphysics of Clouds and Precipitation*, Riedel, Boston, MA, 1980.
  - [32] U. RIEBESELL AND D. A. WOLF-GLADROW, *The relationship between physical aggregation of phytoplankton and particle flux: A numerical model*, *Deep. Res.*, 39 (1992), pp. 1085–1102.
  - [33] J. SILK AND S. D. WHITE, *The development of structure in the expanding universe*, *Astrophys. J.*, (1978).
  - [34] L. G. STANLEY AND D. L. STEWART, *Design Sensitivity Analysis: Computational Issues of Sensitivity Equation Methods*, SIAM, 2002.
  - [35] M. P. SURH, J. B. STURGEON, AND W. G. WOLFER, *Void nucleation, growth, and coalescence in irradiated metals*, *J. Nucl. Mater.*, 378 (2008), pp. 86–97.
  - [36] K. THOMASETH AND C. COBELLI, *Generalized Sensitivity Functions in Physiological System Identification*, *Ann. Biomed. Eng.*, 27 (1999), pp. 607–616.
  - [37] S. TULJAPURKAR AND H. CASWELL, eds., *Structured-Population Models in Marine, Terrestrial, and Freshwater Systems*, *Population and Community Biology*, Springer, 1997.
  - [38] M. VAN SMOLUCHOWSKI, *Drei Vorträge über Diffusion, Brownsche Bewegung und Koagulation von Kolloidteilchen*, *Zeitschrift für Phys.*, 17 (1916), pp. 557–571.
  - [39] ———, *Versuch einer mathematischen theorie der koagulation kinetic kolloider losungen*, *Zeitschrift für Phys. Chemie*, 92 (1917), pp. 129–168.
  - [40] J. A. D. WATTIS, *An introduction to mathematical models of coagulation-fragmentation processes: A discrete deterministic mean-field approach*, *Phys. D Nonlinear Phenom.*, 222 (2006), pp. 1–20.
  - [41] R. M. ZIFF AND G. STELL, *Kinetics of polymer gelation*, *J. Chem. Phys.*, 73 (1980), p. 3492.

## Appendix A. Domain choices for aggregation kernels.

The theoretical  $\mathcal{D}$  on which the PGSFs are defined starts at a point  $\mathbf{0} \in \mathbb{R}^N$ . For our purposes, the PGSFs incorporate  $\left(\frac{\partial f}{\partial \alpha}\right)^2$ , so when we examine the lower ends of  $\mathcal{D}$ , we consider the limit as  $t, x \rightarrow 0^+$  of  $\left(\frac{\partial f}{\partial \alpha}\right)^2$ . In this appendix, we determine



$\lim_{t,x \rightarrow 0^+} \left( \frac{\partial f}{\partial \alpha} \right)^2$  for each of the the three coagulation kernels.

For  $K(x, y) \equiv \alpha$ ,

$$f(t, x; \alpha) = \left( \frac{2}{\alpha t} \right)^2 e^{\frac{-2x}{\alpha t}},$$

therefore

$$\frac{\partial f}{\partial \alpha} = \frac{8}{t^2 \alpha^3} e^{\frac{-2x}{\alpha t}} \left[ \frac{x}{t\alpha} - 1 \right].$$

Then

$$\left( \frac{\partial f}{\partial \alpha} \right)^2 = \frac{64}{t^4 \alpha^6} e^{\frac{-4x}{\alpha t}} \left[ \frac{x}{t\alpha} - 1 \right]^2,$$

therefore

$$\lim_{(t,x) \rightarrow (0^+, 0^+)} \left( \frac{\partial f}{\partial \alpha} \right)^2 = \lim_{(t,x) \rightarrow (0,0)} \frac{64}{t^4 \alpha^6} e^{\frac{-4x}{\alpha t}} \left[ \frac{x}{t\alpha} - 1 \right]^2,$$

which does not exist. Choosing the path  $x = 0$  demonstrates the infinite limit,

$$\begin{aligned} \lim_{(t,0) \rightarrow (0^+, 0^+)} \left( \frac{\partial f}{\partial \alpha} \right)^2 &= \lim_{(t,0) \rightarrow (0^+, 0^+)} \frac{64}{t^4 \alpha^6} e^{\frac{-4x}{\alpha t}} \left[ \frac{x}{t\alpha} - 1 \right]^2 \\ (A.1) \qquad \qquad \qquad &= \lim_{(t,0) \rightarrow (0^+, 0^+)} \frac{64}{t^4 \alpha^6}. \end{aligned}$$

The infinite limit in (A.1) helps guide our choice of  $\underline{t} = 0.2$  for  $\mathcal{D}$ , which ensures our PGSFs calculations remain within computer precision.

For  $K(x, y) \equiv \alpha(x + y)$ ,  $\alpha \in \mathbb{R}_+ < \infty$ ,  $x \in (0, \infty)$ ,  $t \in [0, \infty)$  and as adapted from [28],

$$(A.2) \qquad f(t, x; \alpha) = \frac{1}{\sqrt{2\pi}} x^{-3/2} (e^{-\alpha t}) e^{-x/(2e^{2\alpha t})},$$

where it naturally follows that

$$f(0, x; \alpha) = \frac{1}{\sqrt{2\pi}} x^{-3/2} e^{-x/2}.$$

As we choose  $\mathcal{D}$  for the additive kernel, we again consider

$$\lim_{(t,0) \rightarrow (0^+, 0^+)} \left( \frac{\partial f}{\partial \alpha} \right)^2$$

and note

$$\left( \frac{\partial f}{\partial \alpha} \right)^2 = \frac{t^2 e^{-2\alpha t} e^{(-x e^{-2t})}}{2\pi x^3}.$$

Then for any  $t = a$ , where  $a$  is constant strictly greater than zero,

$$\lim_{x \rightarrow 0^+} \left( \frac{\partial f}{\partial \alpha} \right)^2 = \lim_{x \rightarrow 0^+} \frac{a^2 e^{-2\alpha a} e^{(-x e^{-2a})}}{2\pi x^3},$$

which is infinite. Choosing  $\underline{x} = 0.1$  as our minimum value ensures our PGSFs calculations remain within computer precision.

For  $K(x, y) \equiv \alpha xy$ ,  $\alpha \in \mathbb{R}_+ < \infty$ ,  $x \in (0, \infty)$ ,  $t \in [0, 1)$  and as adapted from [28],

$$(A.3) \quad f(t, x; \alpha) = \frac{1}{\sqrt{2\pi}} x^{-5/2} e^{-(1-\alpha t)^2 x/2},$$

where it naturally follows that

$$f(0, x; \alpha) = \frac{1}{\sqrt{2\pi}} x^{-5/2} e^{-x/2}.$$

As we choose  $\mathcal{D}$  for the multiplicative kernel, we again consider

$$\lim_{(t,0) \rightarrow (0^+, 0^+)} \left( \frac{\partial f}{\partial \alpha} \right)^2,$$

and note

$$\left( \frac{\partial f}{\partial \alpha} \right)^2 = \frac{t^2 e^{(-x(\alpha t - 1)^2)} (\alpha t - 1)^2}{2\pi x^3}.$$

Then for any  $t = a$ , where  $a \in (0, 1)$  is a constant,

$$\lim_{x \rightarrow 0^+} \left( \frac{\partial f}{\partial \alpha} \right)^2 = \lim_{x \rightarrow 0^+} \frac{a^2 e^{(-x(\alpha a - 1)^2)} (\alpha a - 1)^2}{2\pi x^3},$$

which is infinite. Choosing  $\underline{x} = 0.1$  as our minimum value ensures our PGSFs calculations remain within computer precision.